Journal of The Electrochemical Society

Influence of Supporting Electrolyte on Hydroxide Exchange Membrane Water Electrolysis Performance: Anolyte

Journal of The Electrochemical Society, 2021 **168** 084512

Influence of Supporting Electrolyte on Hydroxide Exchange Membrane Water Electrolysis Performance: Anolyte

Aleksandr Kiessling,[1,2] Julie C. Fornaciari,[1,3] Grace Anderson,[1,3] Xiong Peng,[1] Andreas Gerstmayr,[1,2] Michael R. Gerhardt,[1] Samuel McKinney,[4] Alexey Serov,[4] Yu Seung Kim,[5] Barr Zulevi,[4,*] Adam Z. Weber,[1,] and Nemanja Danilovic[1,*,z]**

[1]*Energy Storage and Distributed Resources Division, Lawrence Berkeley National Laboratory, Berkeley, California 94720, United States of America*
[2]*Technical University of Munich, Department of Chemistry, D-85748 Garching, Germany*
[3]*Departments of Chemical Engineering, University of California Berkeley, Berkeley, California 94720, United States of America*
[4]*Pajarito Powder LLC, Albuquerque, New Mexico 87109, United States of America*
[5]*MPA-11: Materials Synthesis and Integrated Devices, Los Alamos National Laboratory, Los Alamos, New Mexico, United States of America*

Hydroxide-exchange-membrane water electrolysis (HEMWE) is an emerging hydrogen-production pathway that combines many advantages of incumbent alkaline water electrolysis (AWE) and proton-exchange-membrane water electrolysis (PEMWE). Advancement in HEMWE has been accelerated with the development of stable and conductive hydroxide exchange membranes (HEMs) and a more comprehensive understanding of alkaline gas-evolving kinetics. However, performance and durability without supporting electrolytes (SELs) remain inferior to PEMWE and AWE and little is known about the role and impact of the SELs. This study investigates the effects of SELs used as anolyte solutions in HEMWEs including cation-type, anion-type, SEL conductivity and pH, presence of carbonates and increased cation/OH^- ratios on cell voltage and stability. We report our findings that (i) cell potential and high-frequency resistance did not correlate with anolyte SEL conductivity, (ii) cation-type influences cell voltage at low current densities (<50 mA cm^{-2}) as predicted by half-cell measurements, (iii) increased cation/OH^- ratio causes increased overpotentials, and (iv) carbonates are exchanged in the HEM but removed via self-purging at high current density. Overall, this study concludes that concentrated KOH is still the best SEL.
 [DOI: 10.1149/1945-7111/ac1dcd]

Manuscript submitted May 20, 2021; revised manuscript received August 6, 2021. Published August 26, 2021.

Supplementary material for this article is available online

The transition to a carbon-neutral economy requires efficient energy-storage technologies.[1,2] Beyond batteries, which excel for short-term power-to-power applications, hydrogen as a chemical energy carrier offers long-term storage capabilities that enable balancing seasonal energy demands in power to X (P2X) applications, including carbon-neutral transportation, heating, food production, and industrial process gas.[1–3] However, the generation of "green" hydrogen, i.e., hydrogen from renewable energy, requires water electrolysis that can dynamically respond to electrical loads, requiring the response to be quick and safe. The traditional alkaline water electrolysis (AWE) is a poor choice due to the presence of a gas-permeable diaphragm separator. This separator does not allow the AWE to operate under differential pressure and low turndown ratio conditions, both of which are advantageous from the perspective of eliminating the cost and safety issues associated with high-pressure oxygen handling.[4] As a result, proton-exchange-membrane water electrolysis (PEMWE) is seen as the preferred technology as it has been demonstrated to overcome these challenges.[5,6] However, scaling PEMWE could be difficult in the gigawatt-terawatt range, if necessary reductions in titanium and rare platinum group metals (PGM) prove to be insurmountable.[4,7–9] Consequently, an emerging technology is hydroxide-exchange-membrane water electrolysis (HEMWE), which can use PGM-free catalysts and cheaper non-titanium stack components, such as stainless steel, while retaining the beneficial aspects of membrane-based technologies.[10] The major challenges for HEMWE are the immaturity of the solid-state ionomers, the requirement for supporting electrolytes instead of liquid water operation for comparable performance to PEMWE, and poor durability.[11] Further the combination of PGM-free and SEL-free HEMWE technology has not been demonstrated at sufficient performance or durability relative to SEL-containing HEMWE or PEMWE.

A HEMWE sketch is shown in Fig. 1, it splits water according to Eqs. 1 and 2.[12]

Hydrogen Evolution Reaction (HER):

$$4\,H_2O + 4\,e^- \rightarrow 4OH^- + 2\,H_2 - 0.82 \text{ vs SHE} \quad [1]$$

Oxygen Evolution Reaction (OER):

$$4OH^- \rightarrow O_2 + 2\,H_2O + 4\,e^- \; 0.40 \text{ vs SHE} \quad [2]$$

However, HEMWE is a less mature technology and many challenges remain, including (i) high overpotentials due to poor hydroxide exchange membrane (HEM) conductivity and sluggish non-PGM kinetics,[13,14] (ii) fast ionomer degradation,[15–17] and (iii) the need to flow caustic electrolytes (supporting electrolytes, SEL) in lieu of de-ionized water (DIW) to achieve acceptable durability and operational performance i.e. small and stable voltages.[18]

HEMs are the crucial component that is currently limiting the performance and durability of HEMWE. HEMWEs are typically operated with only an anode (anolyte) feed to leverage PEMWE systems and ease product separation.[19] The cathode is operated with no water or SEL feed (no catholyte), often termed "dry" operation. Since water is required for both the HER at the cathode (Eq. 1) and ionomer hydration, a dry cathode would be detrimental. Water supply to the cathode is thus attained by diffusion from the anode. Unfortunately, osmotic drag in alkaline conditions drives water from the cathode to the anode. Subsequently, the cathodic HER (Eq. 1) should be understood to be at risk of diffusion limitations and potentially cathode ionomer dryout.[20,21] While cathode SELs (catholytes) may influence performance, these are beyond the scope of this paper; we rigorously study the catholyte effects in our follow-up study.

*Electrochemical Society Member.
**Electrochemical Society Fellow.
[z]E-mail: ndanilovic@lbl.gov

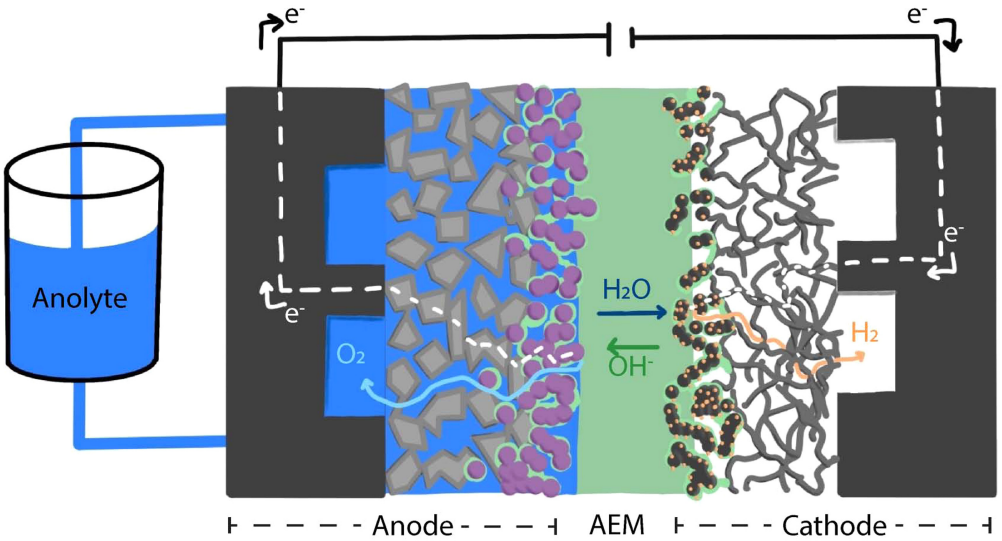

Figure 1. HEMWE sketch; Abbreviations: PTL—porous transport layer, CL—catalyst layer, HEM—hydroxide exchange membrane, anolyte—anodic supporting electrolyte. OER is performed in the anode CL and HER in the cathode CL.

When HEMWEs operate with DIW on the anode side, as is standard operation for PEMWEs, their performance (overpotential) and durability suffer.[1–3] This is mitigated with the use of SELs, regardless of the HEM chemistry chosen; the most commonly used SELs are KOH and NaOH (at concentrations of up to 8 M) and K_2CO_3.[21,22] While detailed mechanistic understanding of SEL effects is lacking, the SEL is hypothesized to: (1) provide additional ion-conducting transport pathways within the pores of the catalyst layer as well as in the HEM ionomer on the anode; (2) The SEL can change the bulk and local pH in the anode catalyst layer; (3) the SEL anions and cations have been shown to affect the electrocatalysis of the oxygen-evolution reaction (Eq. 2) in rotating disk electrode (RDE, half-cell measurements) studies (Eq. 2).[4–7]

Herein, we attempt to determine the role of the anolyte SELs in HEMWE by evaluating the following: is the HEMWE performance influenced by anolyte cation (lithium, sodium, and potassium) or anion effects (hydroxide, carbonate, and nitrate)?; is anolyte SEL conductivity or pH more important for performance?; how does anolyte SEL affect performance vs water? The insights found will be of relevance to the emerging HEMWE community.

Experimental

Cell materials and electrolyte solutions.—Tokuyama A201 membrane (28 μm dry thickness) and AS-4 ionomer were used in this study to allow replicable operation with DIW and SEL. Membrane-electrode assemblies (MEAs) were acquired from Pajarito Powder LLC (PP), Albuquerque, NM, USA, and received as catalyst-coated membranes (CCMs) using Tokuyama A201 and AS-4 ionomer with loadings of $\sim$0.8 mg_{Ir} cm^{-2} IrO_2 ($\sim$150 m^2 gr^{-1}, PP) and 0.5 mg_{Pt} cm^{-2} 50 wt% Pt/C ($\sim$130 m_{Pt}^2 gr^{-1}, PP). CCMs were spray coated using ultrasonic Sono-Tek *ExactaCoat*, loadings and uniformity were characterized by XRF, see SI section 1.3 for detail. Respective AS-4 ionomer-to-catalyst ratios were 10 and 15 wt% for IrO_2 and Pt/C electrodes. MEAs were ion-exchanged to hydroxide form in $\sim$50 ml 1 M KOH at the ambient temperature inside a polyethylene bag for 1 h, rinsed and then mounted into the cell.

Electrolytes were prepared under ambient conditions using Milli-Q water (DIW) and solutes given in Supporting Table I. Electrolytes were stored in PET bottles and exposure to ambient air was limited as much as possible whenever electrolytes were connected to the cell or electrolyte conductivity measurements were taken. Electrolyte conductivity and pH were measured using a Thermo Fischer Scientific *Orion Starr A215* pH/conductivity meter with an *Orion 013005MD* conductivity probe and *Orion 8157BNUMD Ross Ultra pH/ATC* triode. Supporting Fig. 1 (available online at stacks.iop.org/JES/168/084512/mmedia) and Supporting Table II show figures for electrolyte conductivities and correlation parameters, respectively. The self-measured correlations were used to match electrolytes and determine the required concentration for similar conductivity. Throughout the figures in this paper, * denotes similar conductivities and § denotes similar pH at 60 °C.

Cell preparation.—The electrochemical cell used in these experiments was a customized cell procured from NEL Hydrogen (Connecticut, USA), performance was functionally equivalent to the standard Fuel Cell Technologies Inc. (New Mexico, USA) cell. The nominal hardware active area was 25 cm^2, however, we isolated it to 5 cm^2 using gaskets. Platinized-titanium serpentine flow fields were used on the anode and graphitic serpentine flow fields were used on the cathode. PTFE gaskets were used for both anode and cathode to assure the cell was sealed completely. Platinum-coated titanium porous transport layers (PTL, NEL Hydrogen) were used on the anode and carbon gas diffusion layers (Toray, Fuel Cell Store, Texas, USA) were used on the cathode to help SEL and gas transport to the catalyst layers. To assure proper sealing, 3.05 N·m was applied using a torque wrench in incremental $\sim$1 N·m steps. Cells were assembled in ambient air. Components used in cell testing are shown in Supporting Table III.

Cells were connected to a *KNFUSA NFB25 KPOCB-4A* membrane pump at the anode and operated at 5% of maximum pumping power equaling a flow rate of 22 ml min^{-1}. Cells were heated using a *Digi-Sense TC6500* temperature control and heater to a temperature of 60 °C. Heating was never applied when the cell was fully dry but only if there was at least DIW or a supporting electrolyte supplied to the anode side. Electrolytes were indirectly preheated by immersing in beakers and using *VWR* heating plates. The cathode inlet remained closed, while the outlet vented into the fumehood for the duration of the entire experiment. Before SEL experiments began, cells were rinsed with DIW to check for leakage.

Cell testing.—When electrolytes were changed, heating was turned off to prevent severe dry out and the feeding tube was removed from the electrolyte bottle. After the tubing was free of electrolyte, the cell was rinsed with up to 4 batches of 500 ml DIW until the conductivity of rinsing water dropped below 1 μS cm^{-1}. DIW rinsing was omitted when the same or highly similar electrolyte at higher concentrations was subsequently used.

Biologic *VMP3B-10* potentiostats were used for polarization curves (PC) and electrochemical impedance spectroscopy (EIS) with a 10 A current booster. CVs from 1.23 to 2 V at 50 mV s^{-1} were recorded to assess the MEA before polarization curves were recorded. Polarization curves were recorded at constant currents for each MEA. Thereafter, cell voltage was monitored for 2 min before the EIS script was started. EIS was recorded from 1 MHz to 100 mHz with 6 points per decade according to Supporting Table IV. Tests for multiple SELs were run for each MEA; to assure MEA degradation was not substantial, 1 M KOH was tested in between the other electrolytes and its performance was used to quantify degradation. For each of the figures, the numbers in parentheses give the series of test execution. Intermediate KOH curves, from the test series, were omitted whenever they did not provide any additional insights and decreased plot clarity. As experiments were replicated with several MEAs, the Supporting Information shows results of the respective replica. We caution that due to the sequential experiment execution, the data obtained shows qualitative trends, and HFR and voltages between different figures should not be compared.

Polarization curves were recorded at 60 °C after some pre-electrolysis to remove any trapped gas or contaminant species in the cell. Respective currents are shown in Supporting Table IV, along with whether subsequent EIS was recorded. Typical equilibration time was approximately 2 min, but the time was altered if it was observed that cell voltage did not level off within the 2 min. This time alteration was necessary for the case for nitrate and carbonate-containing electrolytes or hydroxide at very low concentrations. For DIW, only currents for voltages $<\sim$1.85 V were investigated, and polarization curves were usually terminated around 120 mA cm^{-2}. Data wer processed using MATLAB. EIS data was automatically fitted to a R-RQ-RQ circuit using the ZFit MATLAB script found online[23] and fits achieved good results.

Results and Discussion

DIW operation.—Ideally, HEMWE would operate on pure water. While the Tokuyama A201/AS-4 system used in this study is a relatively old technology,[24] it is the most studied and often compared with emerging HEM systems (Fumion, Sustanion, Ionomr (AEMION), Orion, Versogen (PIPERION), LANL, and Georgia Tech (PENTION)[1,18,22,25,26]). Operating with DIW solely utilizes catalyst sites covered with the HEM ionomer, in our case AS-4. However, in all cases, when HEMWEs operate with DIW, their performance (overpotential) suffers while durability in either case of SEL or DIW is a challenge that is being addressed with new materials.

We show this tradeoff for Tokuyama MEAs in Fig. 2, where we compare DIW and 1 M KOH anolytes. Note that we will refer to current ranges from 0 to 50 mA cm^{-2} as kinetic region and from 250 to 2000 as ohmic region, throughout the paper.

First, the performance of the 1 M KOH HEMWE is nearly equivalent to PEMWE operation on Nafion™ 117 (N117), achieving roughly 2 A cm^{-2} below 2V.[27] Next, after adequate circulation of DIW as an anolyte, a polarization curve was obtained, there is a $\sim$150 mV penalty at 250 mA cm^{-2} and high current densities are not sustainable as with SELs. The inset in Fig. 2 shows that the kinetics of the reaction are severely affected, with a 150 mV overpotential increase, which can be attributed to a combination of reaction mechanisms (based on the slope change) and electrochemically active surface area changes. Supporting Fig. 3 shows the HFR and polarization resistance obtained during the testing, both the polarization and the HFR are much higher while operating in DIW. Interestingly the ohmic resistance decreases with increasing current density, starting to approach the KOH anolyte condition, one would expect the opposite trend in ohmic resistance, if dehydration of the polymer were occurring at higher current densities with electro-osmotic drag. It appears that there is a concomitant increase in hydroxide concentration that increases the membrane conductivity.

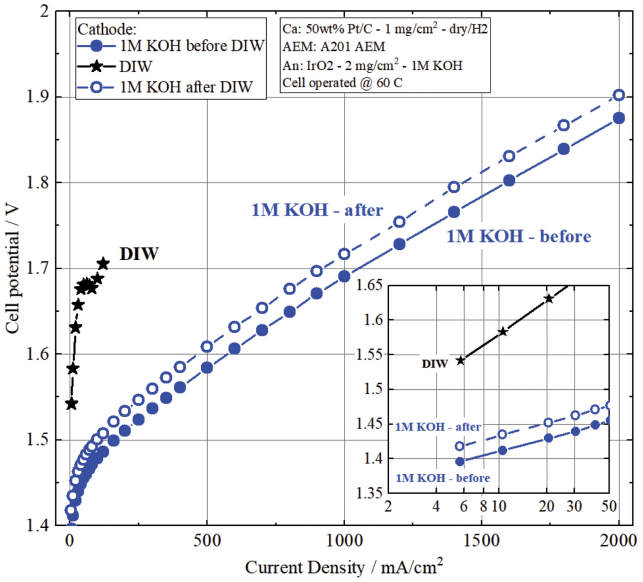

Figure 2. Polarization curves showing kinetic (inset, Tafel plot) and ohmic regions for DIW and KOH anolyte. One observes much higher cell voltages for DIW than 1 M KOH anolyte. Current density range of DIW was limited so that HEM degradation remained minor. However, even in relative terms small DIW operation resulted in substantial degradation as can be seen by comparing the 1 M KOH before and after DIW operation.

However, it is not enough to overcome the kinetic limitation. After operating on DIW and returning to 1 M KOH operation, there is irreversible degradation in the polarization curve, suggesting that the onset of degradation is swift, even though the voltage and current used to operate on DIW were low and cumulative capacity throughout was much smaller than for 1 M KOH. While rigorous durability assessment is beyond the scope of our study, it has been suggested that the durability of AEMWEs is affected not only by alkaline stability but also the electrochemical stability of AEM and ionomer.[28,29] Clearly an SEL is important at least with this polymer/ionomer materials set, to overcome kinetic limitations, presumably imposed solely at the anodic side of the cell. We now look at how the choice of anode SEL changes the cell operating characteristics by separating out cation and anion effects. We also attempt to determine why the cell functions better with an anolyte SEL.

Cation effects.—Recent progress in the understanding of the alkaline OER mechanism on PGM and PGM-free catalysts (overpotentials for PGM-free and Ir-based catalysts tend to be very close to each other[13]) has focused on the influence of cation effects from aqueous electrolytes using RDE (half-cells), and has shown that cations stabilize adsorbed hydroxide (OH*) through non-covalent interactions, leading to a decrease in OH^- mobility in the interfacial double layer and leading to a corresponding decrease in OER activity.[14,30,31] The stabilization strength follows the charge density of the cation following the trend from $K^+ < Na^+ < Li^+$. These types of ion effect studies have yet to be studied in full-cells (HEMWE), one would expect a direct comparison between half-cells and full-cells to result in decreasing performance for SELs with increasing stabilization strength KOH < NaOH < LiOH.

We evaluate the influence of the cation type at the same cation concentration, 1 M, and at the same SEL conductivity as for 1 M KOH at 60 °C as shown in Fig. 3. We found the equivalent conductivities with 1 M KOH ($\sim$333 mS cm^{-1} at 60 °C), to be 1.45 M LiOH and 1.23 M NaOH (SI Fig. 1). We compare the trend between K^+ and Li^+ first, followed by K^+ and Na^+. We emphasize again since there is variation in the as prepared MEAs, there is an initial KOH performance variance (Figs. 3a vs 3b). Therefore, we compromise in how these experiments were performed, and how

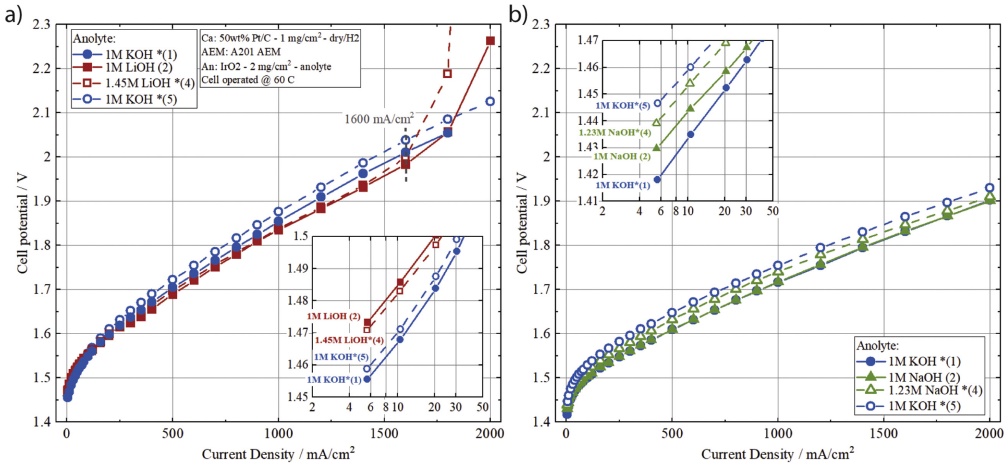

Figure 3. Polarization curves showing kinetic (inset Tafel plot) and ohmic regions for KOH, LiOH (a) and KOH, NaOH (b) anolytes. Numbers in brackets indicate the series in which the experiments were conducted consecutively, * denotes similar conductivities at 60 °C. For (a) 1 M and 1.45 M LiOH, points from 1600 mA cm^{-2} do not represent a steady state.

they should be interpreted; comparing effects within a series on one MEA is appropriate (K^+ vs Li^+ in one series), however, comparing effects between series on multiple MEAs is most likely inappropriate (Na^+ vs Li^+). Similarly using error bars would be erroneous, thus we opt to show reproducibility of the effect within a series in the SI.

The polarization curves (PCs) in Fig. 3a show the kinetic and ohmic regions for LiOH and KOH anolytes. As one can see in the inset for the kinetic region, higher voltages were observed for LiOH than for KOH at the same concentration and SEL conductivity. The increased voltage for LiOH in the kinetic region matches with the expected stabilizing effect of Li^+ on OH*. However, PCs show lower voltages for LiOH than for KOH in the ohmic region, from 200 to 1400 mA cm^{-2} at the same concentration and SEL conductivity. 1.45 M and 1 M LiOH showed similar PC traces although SEL conductivity varied by 79 mS cm^{-1}. As one can see in SI Fig. 4, this effect was observed for several datasets and different MEAs. For currents higher than 1600 mA cm^{-2}, cell voltages are higher for LiOH than for KOH. Looking at the HFR in SI Fig. 5 an increasing HFR at high current density is observed for both Li-containing electrolytes, while general HFR trends appear to follow the SEL conductivity at intermediate current densities. Note there is no significant effect of cation type on the polarization resistances at intermediate current densities, implying that the local shielding effects of the anion remain in the 10 mV range (Fig. 3a inset), however at the upper end of the current range spikes in polarization resistance of Li containing electrolytes are seen. We further note that the LiOH PC data points do not represent a steady-state as a steady reversible voltage increase was observed as shown in SI Fig. 6.

We hypothesize that the steady voltage increase, and the increasing HFR at high current densities for both K^+ and Li^+, thus cations inhibit the water supply to the HEM (inhibition of water transport through the membrane). Table I shows the hydration-free enthalpy, solubility at 60 °C, and exchange time of a water molecule in a hydration shell for relevant cations. One can see that the exchange time and hydration-free enthalpy for Li^+ is higher than for Na^+ and K^+ while LiOH has a significantly smaller solubility than NaOH and KOH. The work of Stanislaw et al.[32] shows that hydroxide concentrations close to the HEM may reach up to 10 mol L^{-1}, exceeding the solubility of LiOH at 60 °C.[33] Recently, precipitation of potassium bicarbonate at the cathode was modeled for CO_2 electrolysis cells employing alkaline electrolytes as anode SELs.[34] Thus, we hypothesize that LiOH precipitates close to the anode side of the HEM and the precipitate inhibits the water supply to the HEM. Further the polarization resistance spikes at high current density indicate that there is further inhibition of electrocatalytic site access due precipitates forming in the vicinity of the reaction sites. Post-testing visual analysis did not indicate the presence of any participates, likely due to the final KOH test performed to test degradation. We emphasize that the water uptake of the HEM may also change as a result of the SELs used, as well as the conductivity of the HEM being affected by both the SEL and the dehydration, the characterization of which was beyond the scope of this paper. In any case, this induces concomitant effects, as the inhibition will lead to further water being taken from the HEM since the cathode continues to consume water and the overpotential increases due to both drying of the HEM and increasing anodic overpotentials due to active area reduction (similar to the DIW case). Over time, the HEM's water content and conductivity decreases, which is observable as the HFR increases (Supporting Fig. 4). Short-term, HEM dehydration should be recoverable, and should not be present in a subsequent KOH polarization curve. As KOH has also a much higher solubility, there should be no precipitant inhibiting the water uptake, which is in agreement with Fig. 3a. Examining Nyquist plots in Supporting Fig. 7 and HFR in Supporting Fig. 5, strong shifts to higher Re(Z) (i.e. HFR increases) are observed for LiOH at increasing current densities. For KOH, Supporting Fig. 5, shows that HFR was also increasing for KOH at current densities ~1000 mA cm^{-2}, although by <2 mOhm cm^2 per ~1000 mA cm^{-2}, hence dehydration was present for KOH but to a smaller magnitude. From an operational perspective, this means that at high current densities, some water vapor or SEL should be fed to the cathode to prevent HEM

Table I. Radius and volume of an ion with hydration shell r_{hyd} and V_{hyd}, number of hydrate water molecules n_{H2O}, hydration free enthalpy $\Delta_{hyd}G$,[35] solubility of MOH in water at 60 °C[33] and exchange time of water in hydration shell in M-Cl solution τ_{H2O}.[36]

Ion (M)	r_{hyd}/nm	V_{hyd} nm^{-3}	n_{H2O}/–	$\Delta_{hyd}G$/kJ mol^{-1}	Solubility /mol l^{-1}	τ_{H2O}/ps
Li^+	0.241	0.059	5.2	−475	~6.4	35.2
Na^+	0.218	0.043	3.5	−365	~52	26.4
K^+	0.212	0.040	2.6	−295	~25	22.1
OH^-	0.212	0.040	2.7	−430	—	—

Table II. Comparison of kinetic overvoltage at 10 mA cm^{-2}.

SEL	Overvoltage (mV) at 10 mA cm^{-2}[a)]	SEL conductivity (mS cm^{-1})
1 M KOH	0	333
1 M NaOH	10	286
1 M LiOH	20	254

a) Relative to KOH in experimental sequence.

dehydration. We investigate the cathodic hydration impact in our forthcoming catholyte study.

With respect to the better performance for LiOH in the ohmic regime, from 250 to 1600 mA cm^{-2}, than for KOH, we hypothesize that this is due to higher mobility of OH^- in the Li^+-interfacial double layer (IDL) than in the K^+-IDL. Lee et al.[37] reported that in the vicinity of charged surfaces at current densities > 250 mA cm^{-2}, concentrated electrolytes behave like ionic crystals with Schottky defects. Thus, the conductivity of an IDL would be dependent on its defect density which is increased when ions of different sizes are present in the IDL. As one can see in Table I, radii for hydrated Li^+ (0.241 nm), K^+ (0.218 nm), and HO^- (0.212 nm) vary significantly. This yields differences of ~50% for the volume of a hydrated ion.[24] Thus, a Li^+ IDL should have a higher defect density and ionic mobility, which should result in smaller overpotentials necessary to move a charge through a Li^+-IDL than a K^+-IDL.[37] Consequently, HFR-free cell voltages are smaller for LiOH than KOH SELs, which is observed in Supporting Fig. 8. We hypothesize that Li^+ improves performance in the ohmic region compared to KOH due to higher OH^- mobility in the IDL but more work in specifically addressing this phenomenon in the community is warranted.

Next we compare corresponding NaOH anolytes with KOH in Fig. 3b. In the kinetic region, a decrease in activity is seen with the introduction of Na^+, the magnitude of which is smaller than Li^+ compared to K^+ (Table II for comparison). As expected by half-cell experiments Li^+ and Na^+ impede the OER in the kinetic region compared to K^+.[31] However, in the ohmic region at the same cation concentration, PCs of NaOH and KOH overlap; a subsequent increase in NaOH concentration to match the conductivity of 1 M KOH resulted in a slight degradation (increase) in cell voltage, which was reproduced upon subsequent reintroduction of KOH SEL. In contrast to LiOH at high current densities, a steady reversible voltage increase was not observed. Further examination of the Nyquist plots, HFR and polarization plots, Supporting Figs. 9 and 10 respectively, yields no discernable differences.

Thus based on the cation, anolyte study, in the kinetic region increasing charge density $K^+ < Na^+ < Li^+$ has corresponding decreases in activity in full-cell tests. At higher current densities there are new emerging phenomena that correspond to cation interactions with the catalyst, ionomer, membrane and water that interplay in the observed ohmic and polarization trends and subsequent influence on the degradation of the cells. Based on these results the recommendation is to use K^+ containing electrolytes.

Anion effects.—Based on half-cell measurements, the electrolyte anions also play a role in the OER, thus anions of SEL could also have an impact on the OER in full-cell.[14] At the same time, K_2CO_3 is frequently used as an SEL in HEMWE's, but the role of the carbonate anion on the charge-carrying species in the membrane is poorly understood.[38] Especially compared to HEMFCs where it is detrimental to membrane conductivity. Next, we studied the effects of anions in K^+ containing SELs, KOH, and K_2CO_3. We compare the SELs at the same conductivity and the same pH in order to systematically elucidate the difference between the anions themselves on full-cell performance. To match conductivities, a concentration of 0.5 M instead of 1 M KOH was used because if we had matched for conductivity with 1 M KOH, the K_2CO_3 solubility limit would have been exceeded. Thus, K_2CO_3 at 0.82 M was compared with 0.5 M KOH for nearly equivalent conductivity (189 mS cm^{-1}) but different pH (11.35 and 13.65, respectively) at 60 °C; and with 18 mM KOH at the same solution pH (11.22), but different conductivities (189 and 7.4 mS cm^{-1}, respectively). We note we are not accounting for changes in osmotic pressure or activity, which are beyond the scope of our study.

First, looking at just the effect with a hydroxide anion of decreasing conductivity (and pH) of KOH in Fig. 4a, the cell voltage increased going from 0.5 M to 18 mM KOH. This increase intuitively makes sense, as the SEL's OH^- charge carrying species is decreased. The HFR plot in Fig. 4b also supports this finding, showing an increase in HFR at low current densities that increases

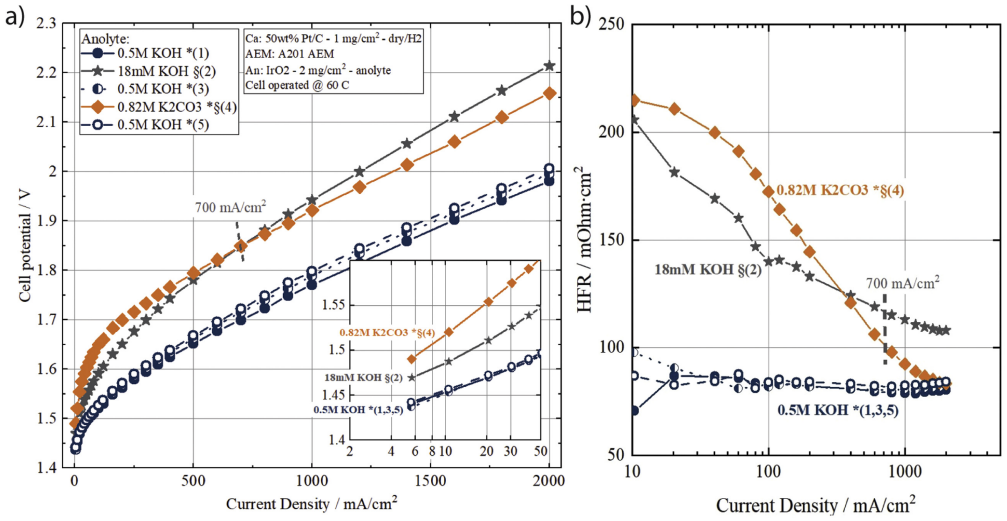

Figure 4. (a) Polarization curve showing the kinetic (inset, Tafel plot) and ohmic regions and (b) HFR resistances; for carbonate and hydroxide solutions. Numbers in brackets indicate the series in which the experiments were conducted consecutively, * denotes similar conductivities and § denotes similar pH at 60 °C.

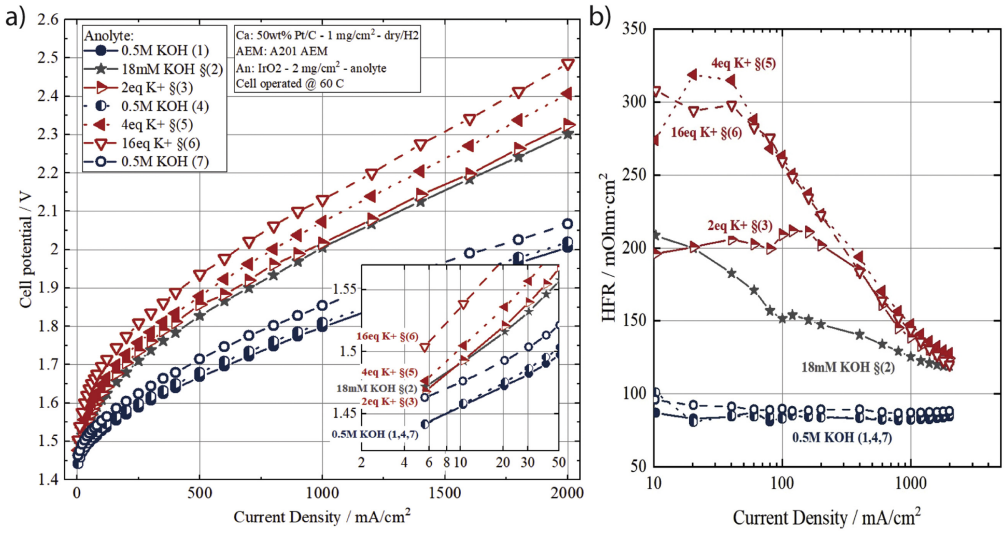

Figure 5. (a) Polarization curve showing the kinetic (inset, Tafel plot) and ohmic regions and (b)) HFR resistances; for anolytes with different cation/OH ratios. [K^+] was increased by adding KNO_3 to 18 mM KOH to obtain cation/OH ratios of 2 (2 eq K^+), 4 (4 eq K^+), 16 (16 eq K^+); 0.5 M KOH is shown for assessment of degradation. Numbers in brackets indicate the series in which the experiments were conducted consecutively, § denotes similar pH at 60 °C.

linearly until it almost matches that of the 0.5 M KOH at higher current density, similar to what was found for pure DIW (Fig. 1). At the same time, the kinetics are slowed, with an almost 50 mV increase corresponding to the pH and conductivity decrease (Fig. 4a inset). Decreasing the pH, regardless of the anion (18 mM KOH and 0.82 M K_2CO_3), decreased the performance. Even though the 0.82 M K_2CO_3 solution conductivity is the same as the 0.5 M KOH. This result implies that the higher pH may have a greater degree of influence on performance over that of solution conductivity, or that there is a secondary effect as the cation/hydroxide ratio is also changing. Comparing the differences between carbonate and hydroxide at the same pH the major difference is in the kinetic region (Fig. 4a inset), where the KOH outperformed K_2CO_3 by 25 mV, this difference is also consistently present at higher current densities in the polarization resistance plot shown in Supporting Fig. 11. The HFR behaved similarly, starting high and decreased with increasing current density for both approaching and matching the higher pH, 0.5 M KOH (Fig. 4b). Examining the PC, the 0.82 M K_2CO_3 is worse than 18 mM KOH at low current, but exceeds the hydroxide SEL at high currents. Since the kinetics of both the low pH SELs remained poor even at a high current density where the HFR matches the 0.5 M KOH, the full-cell performance trend remains. As intermediate and final 0.5 M KOH PCs have voltages in the same range, we think that it is unlikely that degradation plays a major role here.

We hypothesize that there are several effects happening. First the concentration, pH, and conductivity change of the KOH solution results in both kinetic (Tafel region) and polarization (from impedance at higher currents) loss from a decrease in charge carrying species which allows more access to the electrode area. Secondly, the lower anode SEL conductivity results in a higher HFR of the full-cell. This intuitively makes sense, the lower the hydroxide concentration, and conductivity the lower the full-cell performance. The bicarbonate situation is more complicated, presumably due to two factors, the lower conductivity of the carbonate ion relative to hydroxide, as well as higher cation/OH ratio. We hypothesize that the higher voltages for K_2CO_3 in the kinetic region, as well as higher polarization resistance throughout the current density range are a result of the cation/OH ratio. At the starting conditions, for 0.82 M K_2CO_3 cation/OH ratio equaled 95 while for KOH it is 1. We investigate this effect in the following section. Secondly, even though the conductivity of the carbonate SEL is the same as the 0.5 M KOH, there is a significant loss in HFR of the full-cell (Fig. 4b). The HFR improves with increasing current density matching that of 0.5 M KOH. This may be due to due to self-purging effect, discussed later in the manuscript.

To further investigate whether an increase of cation/OH ratio can be related to the observed performance changes we manipulate the cation/OH ratio by adding KNO_3 to maintain the solution pH and increase the SEL conductivity. The nitrate will not react with any of the water, unlike carbonates, and provides a more controlled experiment to study the cation/OH ratio effect.[14] We note that the different anions can affect the ionomer and membrane water uptake and conductivity, the mobilities and affinities for opposing ions will also be different, as reported for other systems.[34,39] The incorporation of these effects is beyond the scope of this paper. However, it is likely that NO_3^- will ion-exchange into the HEM as observed for CO_3.[2–34] In Fig. 5a, we show the effect of potassium nitrate addition to 18 mM KOH in amounts of 1, 3 and 15 equivalents so that cation/OH (resp. K/OH^-) ratios of 2, 4 and 16 were obtained, respectively. The anolyte conductivity increased from 7.4 to 70.5 mS cm^{-1}, while pH remained constant at 11.35. Increased cation/OH ratios are labeled with the total number of equivalents of K^+ per equivalent of OH^-, except for 1, which was labeled as 18 mM KOH.

Kinetic regions in Fig. 5a show higher voltages for increased cation/OH ratio. The same was observed for the ohmic region and polarization resistance (SI Fig. 14). The expected correlation of cell performance with anolyte conductivity was not observed, as shown in Fig. 5b, the HFR increased with increasing cation/OH ratio (while the solution conductivity increased). We note that after the highest cation/OH ratio SEL was used, the MEA showed higher overpotential indicating degradation upon taking a PC in base KOH (open circle curve in Fig. 5, scan 7 in series).

In Table III, we summarize for DIW, OH^-, CO_3^{2-} and NO_3^- anions the SEL conductivity, kinetic overpotential (10 mA cm^{-2}), and HFR at fixed currents of (100 mA cm^{-2} and 1 A cm^{-2}), assuming this represents a steady-state OH^- flux across the membrane in order to differentiate between two effects: kinetic stabilization of OH* (low current) vs site access issues at higher current densities due to anion build up limiting OH^- (high current). We discuss these two separately below. We note that the assumption of a steady-state OH^- flux, is complicated by the presence of carbonate which we have shown to be present in the membrane, so this should only be used as a rough comparative guide.

Impact of the cation/OH ratio on kinetics.—The increased kinetic voltages, of up to 100 mV for high cation/OH ratios (CO_3^{2-} and NO_3^-) irrespective of SEL conductivity, was nearly the same as

Table III. Comparison of SEL conductivity, kinetic overvoltage at 10 mA cm^{-2}, full-cell HFR at 100 mA cm^{-2} and 1 A cm^{-2}.

SEL	SEL Conductivity (mS cm^{-1})	Overvoltage (mV) at 10 mA cm^{-2}[a)]	HFR at 100 mA cm^{-2} (mOhm cm^2)	Cell Voltage (V) at 1 A cm^{-2}	HFR at 1 A cm^{-2} (mOhm cm^2)
DIW	5.5 x 10^{-5}	160	300	n/a	n/a
0.5 M KOH	190	0	75	1.78	75
18 mM KOH	7.4	25	150	1.97	125
0.82 M K_2CO_3	190	80	175	1.93	75
2 eq K^+ (NO_3^-)	7.6	40	210	2.0	140
4 eq K^+ (NO_3^-)	21.5	60	260	2.07	140
16 eq K^+ (NO_3^-)	70.5	90	260	2.12	140

a) Relative to KOH in experimental sequence.

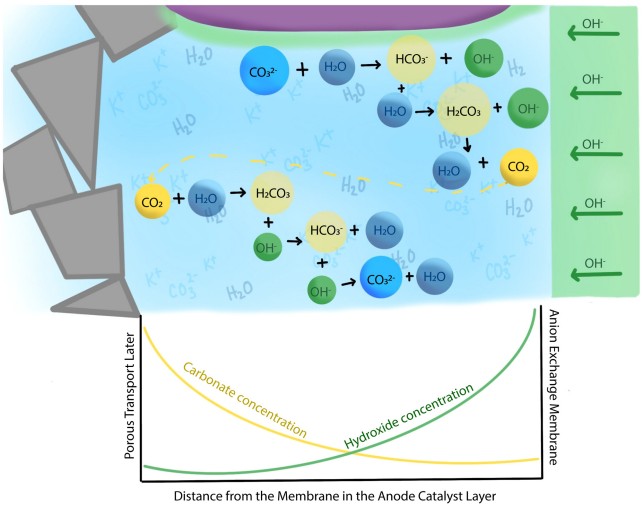

Figure 6. Qualitative concentration profiles of carbonates and hydroxides within the HEM anode catalyst layer.

when DIW was used as SEL. Strongly suggesting that the cations stabilized OH* and thus slowed down OER. To further elucidate these effects, we performed microelectrode-based half-cell measurements in carbonate and hydroxide solutions on an Ir metal microelectrode, shown in Supporting Fig. 17. In these measurements, no alkaline ionomer is present and kinetic response of Ir in varying solutions can be examined similar to the full-cell measurements we performed. The OER activity was primarily controlled by the solution pH, namely at pH ~11, 0.018 M KOH and 0.8 M K_2CO_3 had the same OER activity, while increasing pH up to 14 for 1 M KOH resulted in ever-increasing OER activities. These results suggest that the full-cell findings for carbonate and cation/OH ratio go beyond simple interactions between the electrocatalyst and solution, but maybe dependent on HEM effects as well.

Impact of the cation/OH ratio on transport.—As current increases, the Ohmic resistance can change due to self-purging of CO_3^{2-} and NO_3^-. This self-purging effect occurs at high current densities, when the high hydroxide flux removes other anions (e.g. CO_3^{2-} and NO_3^-) from the HEM at the anode and replaces them with hydroxide from the cathode.[34,39] The result is a recovery of high HEM conductivity and a decrease in HFR (summarized in Table III).[19,24] At high current, the HFR decreases for CO_3^{2-} and NO_3^-, however only the CO_3^{2-} matches the 0.5 M KOH HFR, while remaining more than twice as high for NO_3^-. This is because CO_3^{2-} can be removed from the anode SEL after self-purging by forming CO_2 via Eqs 3 and 4.

Carbonate:

$$CO_3^{2-} + H_2O \rightarrow HCO_3^- + OH^- \quad [3]$$

Bicarbonate:

$$HCO_3^- + H_2O \rightarrow H_2CO_3 + OH^-, \quad [4]$$

Additionally, local pH can change due to the pH dependence of both equations. The change in local pH can yield more CO_2 as time increases. CO_2 may then follow the oxygen gas flux towards the PTL end of the electrode. This mechanism dissipates the accumulation of CO_3^{2-} near the electrochemical interface at the anode allowing faster OH^- flow (depicted in Fig. 6). This might have kinetic implications as well, since the CO_2 evolution could affect the kinetics at reaction sites for OER, i.e. why the polarization resistance is three times higher than OH^- at the same flux through the membrane supporting a lower cell voltage. Whereas NO_3^- has no pathway for removal and accumulates at the interface slowing OH^- flow through repulsion and ensuring a concentration gradient would drive NO_3^- into the membrane through back diffusion (SI Fig. 18).

Conclusions

Herein, we report the results of a detailed anolyte SEL investigation in a HEMWE setup containing different cations and anions, at different concentrations (cation/OH ratio), and at the same SEL conductivity or pH. For cation effects, we observed that Li^+ and Na^+ cations resulted in voltage decay and degradation, which agrees with the reported RDE observations since OH* stabilization slows down kinetics, thus we recommend using K^+ cations in SELs. For anions effects, we observed that performance did not correlate solely with SEL conductivity or pH. Carbonates were kinetically worse than hydroxides due to effects of increased cation/OH and only outperformed at the same pH and at high current densities due to a self-purging effect. We use NO_3^{2-} anions to help unravel the two effects. Demonstrating that increased cations/OH ratio impact the reaction kinetics, even with increasing conductivity of the SEL at a fixed pH. While the inertness of NO_3^{2-} prevented the HFR benefits of self-purging.

From an operational point of view, anode SELs containing, pure, concentrated KOH showed the highest stability and lack of side reactions or other complicating factors that might emerge with intermittent operation. If a reduction in alkalinity is a priority for widespread use, carbonates would be a superior choice if operated at steady-state and high current densities. Durability and stability impacts emerging as a result of cation and anion effects or SEL selection, and changes to membrane and ionomer chemistry and properties were outside the scope of this work.

Acknowledgments

A.K. gratefully acknowledges funding from the German Fulbright Commission and the Studienstiftung des deutschen Volkes. A.K. thanks the Office for International Education for continuous support during this stay in the US and Prof. Hubert Gasteiger for fruitful discussions. N.D., M.R.G., X.P., A.Z.W., J.F., Y.S.K. and G.A. gratefully acknowledge research support from the HydroGEN Advanced Water Splitting Materials Consortium, established as part of the Energy Materials Network under the U.S. Department of Energy, Office of Energy Efficiency and Renewable Energy, Hydrogen and Fuel Cell Technologies Office, under Contract Number DE-AC02–05CH11231 (LBNL) and 89233218CNA000001 (LANL). JCF thanks the National Science Foundation (grant DGE 1106400) for support. S.M., B.Z. and A.S. also acknowledge Advanced Research Projects Agency-Energy under contract DE-AR000688. The authors would like to thank Nel Hydrogen for supplying titanium porous transport layers.

ORCID

Julie C. Fornaciari https://orcid.org/0000-0002-0473-2298
Grace Anderson https://orcid.org/0000-0002-2723-5024
Xiong Peng https://orcid.org/0000-0001-8737-5830
Michael R. Gerhardt https://orcid.org/0000-0002-1272-3607
Alexey Serov https://orcid.org/0000-0003-3182-4726
Yu Seung Kim https://orcid.org/0000-0002-5446-3890
Barr Zulevi https://orcid.org/0000-0003-1696-945X
Adam Z. Weber https://orcid.org/0000-0002-7749-1624
Nemanja Danilovic https://orcid.org/0000-0003-2036-6977

References

1. R. Abbasi et al., *Adv. Mater.*, **31**, 1805876 (2019).
2. M. Felgenhauer and T. Hamacher, *Int. J. Hydrog. Energy*, **40**, 2084 (2015).
3. M. Schalenbach, A. R. Zeradjanin, O. Kasian, S. Cherevko, and K. J. Mayrhofer, *Int. J. Electrochem. Sci.*, **13**, 1173 (2018).
4. I. Vincent and D. Bessarabov, *Renew. Sustain. Energy Rev.*, **81**, 1690 (2018).
5. A. T. Mayyas, M. F. Ruth, B. S. Pivovar, G. Bender, and K. B. Wipke, *Manufacturing Cost Analysis for Proton Exchange Membrane Water Electrolyzers* (National Renewable Energy Lab. (NREL), Golden, CO United States) (2019), (https://osti.gov/biblio/1557965).

6. M. Carmo, D. L. Fritz, J. Mergel, and D. Stolten, *Int. J. Hydrog. Energy*, **38**, 4901 (2013).
7. M. R. Kraglund, M. Carmo, G. Schiller, S. A. Ansar, D. Aili, E. Christensen, and J. O. Jensen, *Energy Environ. Sci.*, **12**, 3313 (2019).
8. W. E. Mustain, *Curr. Opin. Electrochem.*, **12**, 233 (2018).
9. Z. Taie, X. Peng, D. Kulkarni, I. V. Zenyuk, A. Z. Weber, C. Hagen, and N. Danilovic, *ACS Appl. Mater. Interfaces*, **12**, 52701 (2020).
10. J. Parrondo, C. G. Arges, M. Niedzwiecki, E. B. Anderson, K. E. Ayers, and V. Ramani, *RSC Adv.*, **4**, 9875 (2014).
11. K. Ayers, N. Danilovic, R. Ouimet, M. Carmo, B. Pivovar, and M. Bornstein, *Annu. Rev. Chem. Biomol. Eng.*, **10**, 219 (2019).
12. M. David, C. Ocampo-Martínez, and R. Sánchez-Peña, *J. Energy Storage*, **23**, 392 (2019).
13. C. C. L. McCrory, S. Jung, J. C. Peters, and T. F. Jaramillo, *J. Am. Chem. Soc.*, **135**, 16977 (2013).
14. G.-F. Li, M. Divinagracia, M. F. Labata, J. D. Ocon, and P.-Y. Abel Chuang, *ACS Appl. Mater. Interfaces*, **11**, 33748 (2019).
15. D. R. Dekel, I. G. Rasin, and S. Brandon, *J. Power Sources*, **420**, 118 (2019).
16. S. Maurya, A. S. Lee, D. Li, E. J. Park, D. P. Leonard, S. Noh, C. Bae, and Y. S. Kim, *J. Power Sources*, **436**, 226866 (2019).
17. E. J. Park, S. Maurya, M. R. Hibbs, C. H. Fujimoto, K.-D. Kreuer, and Y. S. Kim, *Macromolecules*, **52**, 5419 (2019).
18. Z. Liu, S. D. Sajjad, Y. Gao, H. Yang, J. J. Kaczur, and R. I. Masel, *Int. J. Hydrog. Energy*, **42**, 29661 (2017).
19. J. Peng, A. L. Roy, S. G. Greenbaum, and T. A. Zawodzinski, *J. Power Sources*, **380**, 64 (2018).
20. H. Ito, N. Kawaguchi, S. Someya, T. Munakata, N. Miyazaki, M. Ishida, and A. Nakano, *Int. J. Hydrog. Energy*, **43**, 17030 (2018).
21. I. Vincent, A. Kruger, and D. Bessarabov, *Int. J. Hydrog. Energy*, **42**, 10752 (2017).
22. D. Li et al., *Nat. Energy*, **5**, 378 (2020).
23. J.-L. Dellis, (2021), ZFIT Funct. (https://de.mathworks.com/matlabcentral/fileexchange/19460-zfit) MATLAB Central File Exchange. .
24. B. Pivovar, *2011 Alkaline Membrane Fuel Cell Workshop, National Renewable Energy Lab. (NREL)*, Golden, CO United States (2011), (https://energy.gov/sites/prod/files/2014/03/f12/amfc_may2011_workshop_report.pdf).
25. D. Henkensmeier, M. Najibah, C. Harms, J. Žitka, J. Hnát, and K. Bouzek, *J. Electrochem. Energy Convers. Storage*, **18**, 024001 (1-18) (2020).
26. P. Fortin, T. Khoza, X. Cao, S. Y. Martinsen, A. Oyarce Barnett, and S. Holdcroft, *J. Power Sources*, **451**, 227814 (2020).
27. G. Bender et al., *Int. J. Hydrog. Energy*, **44**, 9174 (2019).
28. B. Pivovar and Y. S. Kim, (2020), 2019Anion Exchange Membrane WorkshopSummary Report., National Renewable Energy Lab. , Golden, CO (United States), NREL/TP-5900-77240 (https://nrel.gov/docs/fy20osti/77240.pdf).
29. D. Li, A. R. Motz, C. Bae, C. Fujimoto, G. Yang, F.-Y. Zhang, K. E. Ayers, and Y. S. Kim, *Energy Environ. Sci.*, **14**, 3393 (2021).
30. D. Strmcnik, K. Kodama, D. van der Vliet, J. Greeley, V. R. Stamenkovic, and N. M. Marković, *Nat. Chem.*, **1**, 466 (2009).
31. J. Suntivich, E. E. Perry, H. A. Gasteiger, and Y. Shao-Horn, *Electrocatalysis*, **4**, 49 (2013).
32. L. N. Stanislaw, M. R. Gerhardt, and A. Z. Weber, *ECS Transactions*, **92**, 767 (2019).
33. P. J. Gierszewski, P. A. Finn, and D. W. Kirk, *Fusion Eng. Des.*, **13**, 59 (1990).
34. L.-C. Weng, A. T. Bell, and A. Z. Weber, *Energy Environ. Sci.*, **12**, 1950 (2019).
35. Y. Marcus, *J. Chem. Soc. Faraday Trans.*, **87**, 2995 (1991).
36. H. Sakuma and K. Kawamura, *Geochim. Cosmochim. Acta*, **75**, 63 (2011).
37. A. A. Lee, C. S. Perez-Martinez, A. M. Smith, and S. Perkin, *Faraday Discuss.*, **199**, 239 (2017).
38. C. C. Pavel, F. Cecconi, C. Emiliani, S. Santiccioli, A. Scaffidi, S. Catanorchi, and M. Comotti, *Angew. Chem. Int. Ed. Engl.*, **53**, 1378 (2014).
39. L.-C. Weng, A. T. Bell, and A. Z. Weber, *Phys. Chem. Chem. Phys.*, **20**, 16973 (2018).